Determination of γ/γ' Lattice Misfit in Ni-Based Single-Crystal Superalloys at High Temperatures by Neutron Diffraction

SHENYAN HUANG, KE AN, YAN GAO, and AKANE SUZUKI

Constrained γ/γ' lattice misfit as a function of temperature (room temperature, 871 °C, 982 °C, 1093 °C, and 1204 °C) is measured by neutron diffraction on the first-generation Ni-based single-crystal superalloy René N4 and second-generation superalloys René N5, CMSX4, and PWA1484. All the alloys studied show negative misfit at temperatures above 871 °C. For René N4, René N5, and PWA1484, the misfit becomes less negative at temperatures above 1093 °C, possibly due to either the chemistry effect or internal stress relaxation. The magnitude of the misfit shows a qualitative agreement with Caron's misfit model based on Vegard's coefficients. The Re-free alloy René N4 was found to have a larger γ lattice parameter and γ/γ' misfit due to higher fractions of Cr, Ti, and Mo. After 100 hours of annealing at high temperatures, René N5 shows a more negative misfit than the misfit after the standard heat treatment.

https://doi.org/10.1007/s11661-017-4455-5

I. INTRODUCTION

THE lattice misfit between γ and γ' phases is one of the critical properties that influence thermal stability and high-temperature mechanical behaviors of Ni-based single-crystal superalloys used in aircraft engines and power generation gas turbines. The lattice misfit between the γ and γ' is defined as

$$\delta = \frac{2(a_{\gamma'} - a_{\gamma})}{(a_{\gamma'} + a_{\gamma})}$$

where a_{γ} and $a_{\gamma'}$ are lattice parameters for the γ and γ' phases, respectively. The γ' precipitates are typically in the range of 60 to 70 vol pct, and their morphology is governed by misfit energy and γ/γ' interfacial energy.[1] When the misfit energy is dominant, the shape of the γ' precipitates changes from spherical to cuboidal and to rodlike with the increase of misfit (absolute value). The misfit is also one of the critical factors controlling γ' coarsening kinetics. The sign of the lattice misfit determines the type of γ' rafting, either P or N, evolved under tensile or compressive creep deformation, and thus affects creep properties.[2] A more negative misfit promotes a finer γ/γ' interfacial dislocation network and increases resistance to dislocation shearing through the γ' precipitates. The misfit is also a sensitive indicator of internal load partition between the γ and γ' phases under different deformation modes.[3] The lattice misfit can be altered by alloy composition, heat-treatment conditions, and temperature, *via* the compositions of the γ and γ' phases, coefficient of thermal expansion, and interface coherency. Determination of lattice misfit is an important step to correlate the evolution of γ' morphology and the mechanical behavior of superalloys.

However, only limited high-temperature misfit data are available in the literature for commercial single-crystal superalloys at their operating conditions, in particular, "constrained" misfit in the heat-treated state without applied loading or prior deformation history. Existing literature data include commercial alloys CMSX2, CMSX4, SRR99, AM1, SC16, and PWA1484[4–21,38–42] and experimental alloys.[22–30,43] This is a small fraction of all the commercial and experimental Ni-based single-crystal superalloys, considering the multicomponent alloy composition space. Some examined the misfit values for cuboidal γ' precipitates after a standard heat treatment for an alloy, while others studied the misfit of rafted γ' precipitates in creep-deformed specimens. Deformation history and γ' morphology are reported to influence misfit value and its temporal evolution. Most experiments were performed at temperatures below 1100 °C, while only a few were between 1100 °C and 1300 °C.[5,7,13,16,19] It is often difficult to compare the literature misfit values because of insufficient information on sample history and lack of measurement and data analysis details.

SHENYAN HUANG, YAN GAO, and AKANE SUZUKI are with the GE Global Research, Niskayuna, NY 12309. Contact email: maxinehuanghsy@gmail.com KE AN is with the Chemical and Engineering Materials Division, Oak Ridge National Laboratory, Oak Ridge, TN 37831.

Manuscript submitted June 29, 2017.
Article published online January 5, 2018

Accurate determination of constrained lattice misfit for single-crystal superalloys is not trivial. The major challenge for misfit measurement by diffraction is angular resolution, as the γ and γ' phases have similar cubic crystal structure and lattice parameters, and most diffraction peaks from the two phases would overlap for misfit values of $\pm$ (0.1 to 0.3) pct. Diffraction peaks unique to the γ' phase, so-called superlattice peaks, are typically very weak for X-ray diffraction. Laboratory X-ray diffraction is inaccurate in measuring lattice misfit, for both polycrystalline and single-crystal superalloys, because of the difficulty in resolving the γ and γ' peaks in the presence of $K_{\alpha 1}$ and $K_{\alpha 2}$ components in the diffraction patterns. High-resolution synchrotron X-ray powder diffraction is most accurate for lattice misfit measurement of polycrystalline materials, but it does not work for single-crystal alloys, as powder diffraction relies on the random orientation of a large number of grains and bulk measurement for constrained misfit does not allow grinding sample into powders. Single-crystal X-ray diffraction can only work on samples of tens of micrometers to a few millimeters in size and, thus, is unfit for samples in the centimeter size range.

We have considered several synchrotron X-ray diffraction techniques but found them unsuitable for our needs. The high-resolution method (10 to 30 keV) with crystal analyzers is designed for polycrystalline materials and can only measure one crystallographic plane a time for single crystals. The high-energy (70 to 100 keV) method in the transmission mode using a two-dimensional detector does not provide better angular resolution than neutron diffraction, and aligning the sample to a Bragg condition with respect to the monochromatic beam is difficult.

After carefully considering all the possible synchrotron and neutron options in the United States, time-of-flight neutron diffraction at the VULCAN beamline,[31] at Oak Ridge National Laboratory, was finally selected as the most ideal technique based on the following considerations:

(1) the neutron can penetrate through the 12 mm-rod samples as is;
(2) the neutron is more sensitive to superlattice peaks than X-ray;
(3) adequate angular resolution to resolve γ/γ' peak overlap;
(4) adequate *d*-spacing coverage (measurement of multiple peaks simultaneously);
(5) the neutron has a large probing volume so that the misfit results are averaged over the dendritic core (DC) and interdendritic region (IDR), with the typical primary dendrite arm spacing between 200 and 500 μm, depending on casting condition, and the chemical segregation between DC and IDR can lead to a difference in chemistry and lattice parameters[9,28];
(6) convenience for sample alignment with respect to both detector banks;
(7) high-temperature capability for large samples; and
(8) simultaneous measurement of lattice strains in two orthogonal directions.

Data analysis, particularly how the lattice parameters of the γ and γ' phases are determined from overlapping peaks, can largely affect the misfit results. Most published work separates the γ and γ' lattice parameters by deconvolution of overlapped peaks using different mathematical functions to describe the peak profile, without considering the position of γ' superlattice peaks. Some published work seems to offer higher fidelity, in which the γ peak positions were determined by either whole pattern fitting of both γ and γ' peaks or single peak fitting with fixed γ' peak position based on superlattice peaks.[11,12,21,24,30] When handling the γ/γ' peak deconvolution, some work uses one peak for the γ matrix, while others use two γ peaks to account for the tetragonal distortion in horizontal and vertical γ channels caused by γ/γ' coherency stress.[10,14,18,22,26–28] All peak fitting procedures come with some constraints on peak widths, intensity ratios related to chemistry, and phase fractions. When the overlapped γ and γ' peaks are symmetrical without a clear shoulder from the γ phase, the single peak fitting procedure may not yield a unique solution. As the γ/γ' peak overlap can vary with both instrumental resolution and sample variations, we recognize that there may not be a "best" peak fitting method for all situations.

In this study, constrained lattice misfits as a function of temperature (up to 1204 °C) are determined by neutron diffraction for the first-generation superalloy René N4 and second-generation superalloys René N5, CMSX4, and PWA1484. Determination of the lattice misfit is critical for establishing correlations between the lattice misfit and mechanical, microstructural behaviors of single-crystal superalloys for future alloy development. Effects of annealing on microstructure evolution and lattice misfit are studied on René N5. Different misfit values along two crystal orientations are briefly discussed.

II. EXPERIMENT

Nominal compositions of the studied alloys are described in Table I. All the alloys were applied the following solution and aging heat treatments on the provided castings by third vendor.

René N4 : 1260 °C/2 hour + 1080 °C/4 hour + 900 °C/4 hour

René N5 : standard solution and age treatment (general electric proprietary information)

CMSX4 : 1311°C/2 hour + 1140 °C/2 hour + 870 °C/20 hour

PWA1484 : 1312°C/1 hour + 1080 °C/4 hour + 704°C/24 hour

Table I. Nominal Composition of the Studied Alloys (Weight Percent)

Alloy	Ni	Cr	Al	Co	Nb	Ti	Mo	Hf	Ta	Re	W
René N4	bal	9.75	4.2	7.5	0.5	3.5	1.5	0.15	4.8	—	6.0
René N5	bal	7.0	6.2	7.5	—	—	1.5	0.15	6.5	3.0	5.0
CMSX4	bal	6.5	5.6	9.6	—	1.0	0.6	0.10	6.5	3.0	6.4
PWA1484	bal	5.0	5.6	10.0	—	—	2.0	0.10	8.7	3.0	6.0

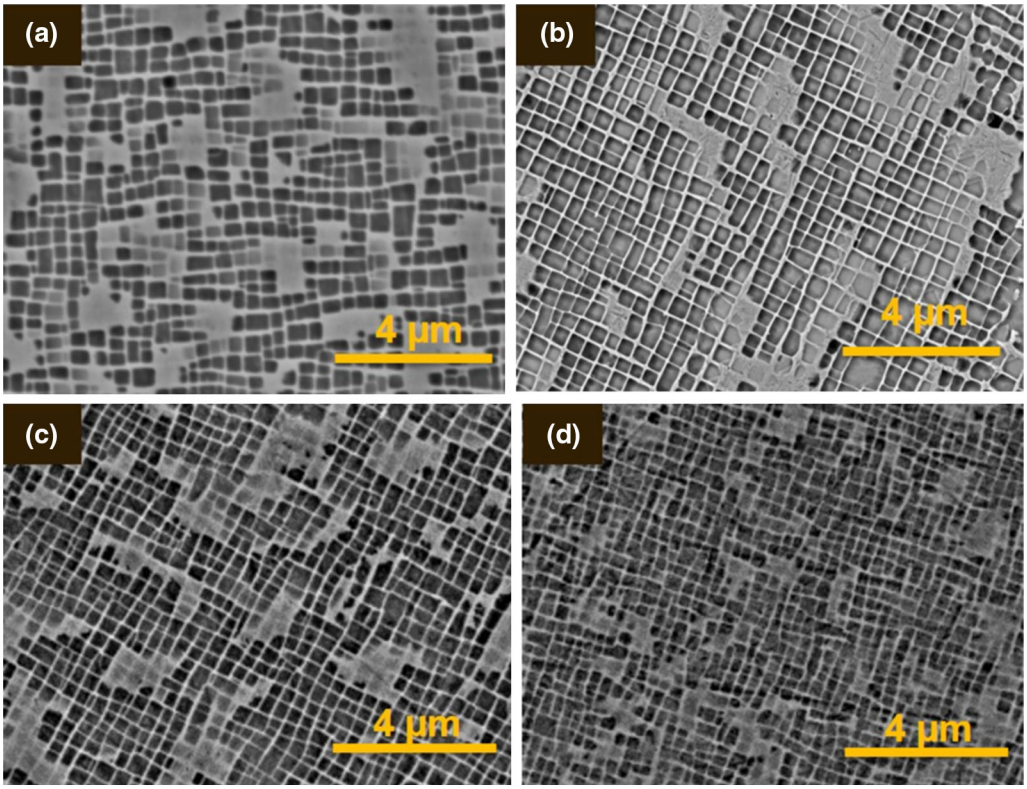

Fig. 1—Backscattered electron images taken from the DC regions before neutron diffraction measurements: (*a*) René N4, (*b*) René N5, (*c*) CMSX4, and (*d*) PWA1484. Dark contrast phase is γ' phase, and light contrast phase is γ phase.

In addition, three René N5 samples were annealed at 982 °C, 1093 °C, and 1204 °C for 100 hours after standard heat treatment to study the annealing effect on lattice misfit.

Neutron diffraction specimens were wired by electrical discharge machining (EDM) and grinded to be cylinders, 20 mm in length and 12 mm in diameter. The axial direction is aligned along the [001] orientation, the dendrite growth direction during casting, within 10 deg of misorientation. To aid the sample alignment at the beamline, one end of the specimen was macroetched to reveal secondary dendrite arms as an indication of [010] and [100] orientations in the transverse direction. Figure 1 shows the representative microstructure of the heat-treated alloys before the neutron measurement. All the alloys reveal cuboidal γ' precipitates with an average size around 300 μm.

Time-of-flight (TOF) neutron diffraction measurements were performed at BL-7, the VULCAN beamline. The experimental setup is shown in Figure 2. The sample was held by spring-loaded alumina rods and heated by the induction heating coils (180 KHz, 5 KW maximum) placed above and below the sample. Two thermocouples were spot welded onto the sample, one in the middle of the gage section as control and readout and the other at 4 mm off-center as readout. The temperature readings of the two thermocouples were stable during the isothermal hold, and the temperature difference across the 4 mm separation was within 10 °C. The sample axial direction is 45 deg from the incident neutron beam. The diffraction data were collected by two area detectors (banks 1 and 2) positioned at ± 90 deg with respect to the incident neutron beam. As the single-crystal samples are oriented along [001], bank 1 collects diffraction patterns from a set of crystallographic planes perpendicular to [001], the axial direction, and bank 2 collects patterns from a set of crystallographic planes parallel to [001], the transverse direction. While the set of planes (001)/(002)/(003)/(004) were always measured by bank 1, the set of planes measured by bank 2 can vary depending upon the sample rotation around its axial direction. For CMSX4,

PWA1484, and standard René N5, (110)/(220) were measured by bank 2, while for René N4 and heat-treated René N5, (100)/(200)/(300)/(400) were measured by bank 2. When an adjacent plane is within 20 deg from these planes, its diffraction peaks can also appear in bank 2, such as (210), (310), and (320). To achieve high angular resolution, the instrument was set at a high-resolution mode ($\Delta d/d = 0.0025$) with chopper speed of 20 Hz. The incident beam slits were 5×5 mm^2, and the irradiated volume was about $5 \times 5 \times 5$ mm^3 defined by both the incident beam slits and the collimators before the detectors. The instrument was calibrated using Si powders inside a 6 mm-diameter vanadium can mounted on the sample stage. The effective d-spacing coverage was between 0.85 and 3.8 Å, including reflections from (100) to (400). Neutron diffraction data were collected at room temperature, 871 °C, 982 °C, 1093 °C, and 1204 °C. Figure 2(d) shows a typical heating profile using induction heating. At each temperature, the sample was held isothermal for 25 minutes. The sample is expected to reach temperature equilibrium during the first 5 minutes, and the data from the remaining 20 minutes were used for analysis.

The diffraction data were analyzed by GSAS to obtain the lattice parameters of both γ and γ' phases. The space groups of γ and γ' are *Fm*-3*m* and *Pm*-3*m*, respectively. The so-called superlattice reflections from γ' are forbidden reflections in *Fm*-3*m* but allowable in *Pm*-3*m*. In other words, the superlattice reflections, such as (100) and (110), have contributions from γ' only, whereas the main reflections, such as (200) and (220), have contributions from both γ and γ'. The diffraction patterns collected in banks 1 and 2 were refined separately. As we are only interested in lattice parameters (*i.e.*, peak positions, not peak intensities), the LeBail method was used, in which the lattice parameters were refined based on peak positions while the peak intensities were allowed to vary to achieve the best fit. The Rietveld method was considered inadequate in this case, as it will fit both peak positions and peak intensities, and the latter depend on the chemical compositions of γ and γ', which are not precisely known.

TOF profile function 3 in GSAS was used, which is most adequate for the VULCAN instrument. The instrumental contributions (based on Si standard powders) are described by a back-to-back exponential function with profile coefficients α, β_1, and β_2, and the sample contribution by a pseudo-Voigt function with profile coefficients σ_1, σ_2 for Gaussian components and γ_1 for the Lorentzian component. In an ideal case, where γ and γ' overlapped peaks can be resolved with sufficient statistics, lattice parameters, Gaussian and Lorentzian components should be refined together without constraints. However, when the misfit is comparable to the

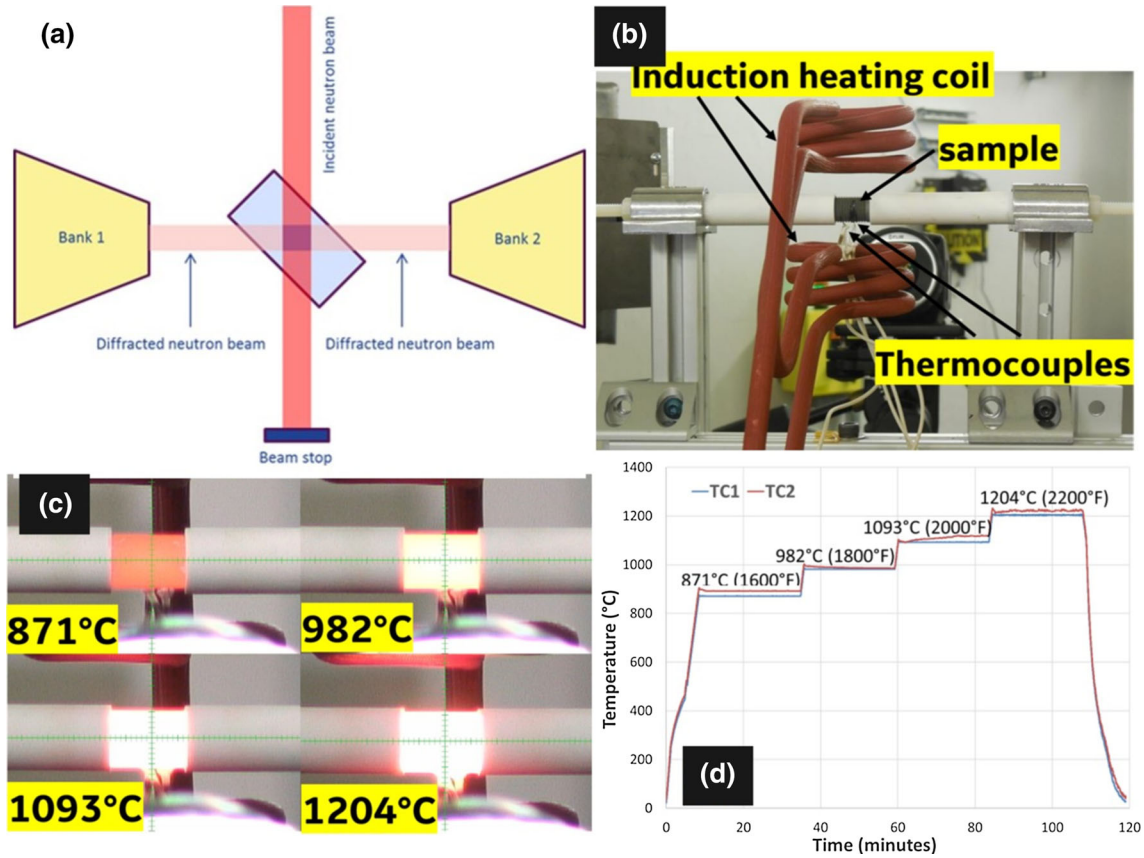

Fig. 2—(*a*) Schematic of the neutron diffraction setup; the sample is at a 45 deg angle with respect to the incident beam, and banks 1 and 2 are two area detectors. (*b*) The sample is held by spring-loaded alumina rods; the heat is provided by the induction heating coils below and above the sample. Control and read-out thermocouples were spot welded onto the middle of the sample. (*c*) The sample is heated to four temperatures. (*d*) Example of heating profile during neutron diffraction measurement.

instrument resolution and the superlattice peak is weak, a special refinement strategy is needed to determine the misfit. In this case, the refinement is based on two diffraction peaks: (100) and (200) for data from bank 1 and (110) and (220) for bank 2. During the refinement, the γ' lattice parameter is fixed based on the superlattice peak position, obtained from refinement with σ_1, σ_2, and γ_1. The γ lattice parameter is refined together with peak profile parameters σ_1 and σ_2 for the γ phase and σ_1, σ_2, and γ_1 for the γ' phase. The Lorentzian components of the γ phase are fixed at values from instrumental contribution. The Lorentzian components for γ cannot be refined without constraining the peak shape parameters between the γ and γ' phases. Fixing or refining the σ_1, σ_2, and γ_1 for γ' makes negligible difference in the γ lattice parameter. Also, it makes a slight difference between refining only Gaussian parameters and refining both Lorentzian and Gaussian parameters for γ, and such difference is greater when peak overlap is more severe. For example, the γ lattice parameter can be changed by 0.002 Å when different refinement schemes are used, and this will lead to a change of the misfit value by 15 pct. Such changes, however, often lead to an overall shift of the misfit *vs* temperature curve. An example of the diffraction pattern and peak fitting results is shown in Figure 3.

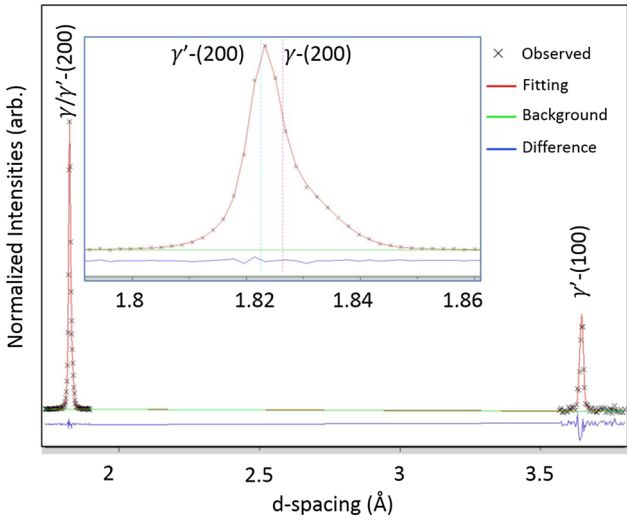

Fig. 3—Example of data analysis on a diffraction pattern collected in bank 1, with a magnified view of the (200) peak. Light blue and magenta dashed lines on the magnified view of the (200) peak represent fitted peak positions of γ and γ' phases, respectively (Color figure online).

As the γ' superlattice peaks do not overlap with the γ peaks, their positions can be accurately determined. Consequently, the accuracy of the misfit is mainly controlled by the accuracy of γ peak positions and that can be affected by γ peak broadening. As the matrix γ phase exits in channels between the γ' precipitates, especially at intermediate temperatures, the γ peak would appear as a broad shoulder next to a sharp γ' peak, and this creates a favorable situation for accurate determination of the γ peak position. When the channels are widened, either at room temperature for certain alloys or at high temperatures for most alloys, the γ peaks become narrowed and the deconvolution between γ and γ' becomes more difficult when the misfit is small. When the magnitude of misfit is between 0.2 and 0.3 pct, the errors are around $\pm$ 0.01 pct. Larger uncertainty ($\pm$ 0.1 pct) of misfit can be seen when the misfit is close to zero, which is the constraint of this instrument resolution.

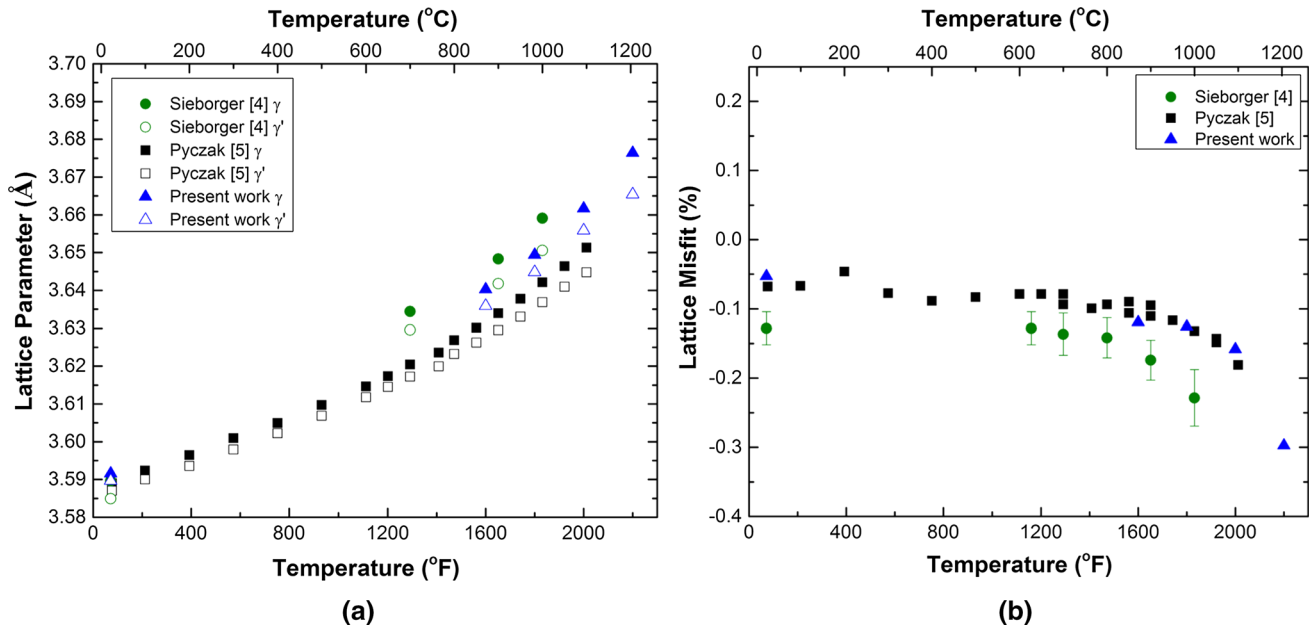

Fig. 4—Comparison of CMSX-4 (*a*) lattice parameters and (*b*) misfit of this study with literature data Reproduced with permission from Refs. [4,5].

III. RESULTS AND DISCUSSION

For a given alloy, the lattice misfit depends on the material condition, but the misfit values can be affected by the measurement technique and data analysis method. Limited literature has reported measurements of the lattice misfit of single-crystal superalloys, and comparisons are made with the data obtained in our present study. Figure 4 presents the lattice parameters and the misfit of CMSX4 as a function of temperature along with the literature data.[4,5] Reference 4 used neutron diffraction, while Reference 5 used X-ray diffraction, and neither of the references provide heat-treatment conditions or the diffraction data analysis method. Our measured lattice parameters are within the range of variation between the reported values in References 4 and 5, and the differences in lattice parameters are within 0.01 Å for the data interpreted for the same temperature. The resulting misfit compares more favorably with Reference 5 than Reference 4. For PWA1484, Lu *et al.*[6] reported the lattice misfit of − 0.13 pct at 900 °C and − 0.3 pct at 1093 °C. Our measured misfits are − 0.47 pct at 871 °C, which shows a large discrepancy, and − 0.27 pct at 1093 °C, which is comparable to the reported value. Possible reasons for the discrepancy may include the following factors: (1) different Ta level in alloy chemistry (9 wt pct in Reference 6 *vs* 8.7 wt pct in the current study) causing different γ, γ' compositions; (2) different heat treatment (single step age in Reference 6 *vs* two-step age in the current study) causing different "starting" compositions of γ, γ' during measurement; and (3) different peak fitting method.

Several trends of misfit behaviors observed from the experiments are summarized in Sections III–A through III–C.

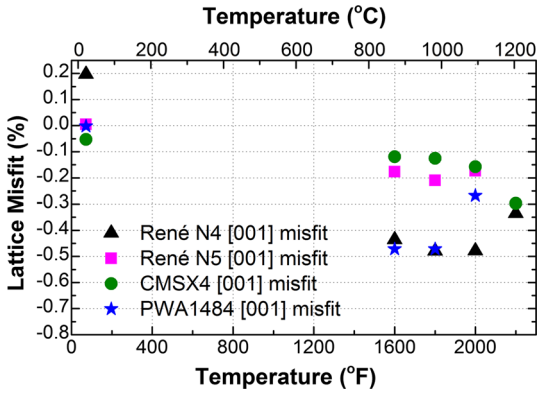

Fig. 6—Lattice misfit as a function of temperature for René N4, René N5, CMSX4, and PWA1484, along the [001] direction (specimen axial direction).

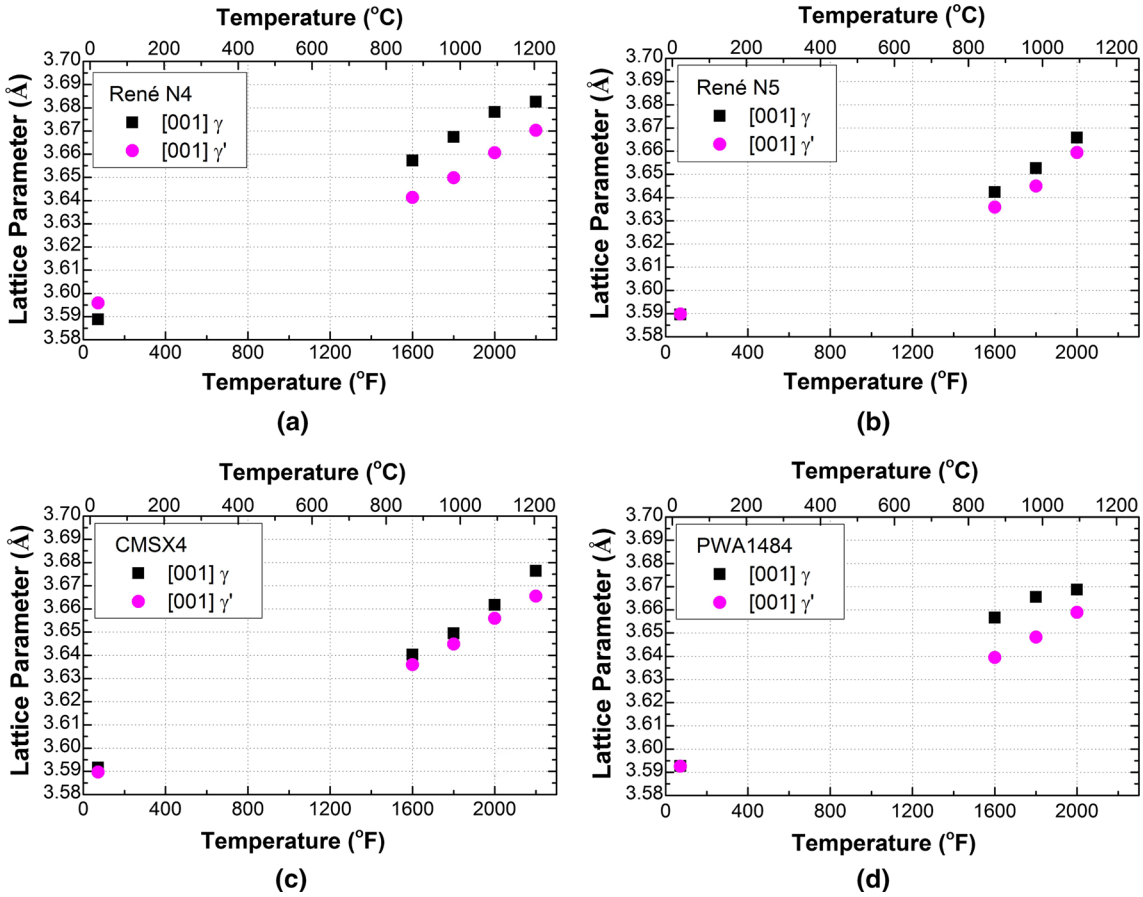

Fig. 5—Lattice parameters as a function of temperature for (*a*) René N4, (*b*) René N5, (*c*) CMSX4, and (*d*) PWA1484, along the [001] direction (specimen axial direction).

Table II. Thermo-Calc Predicted Compositions for the γ and γ' Phases, and Calculated γ and γ' Lattice Parameters Based on Caron's Model,[37] Without Considering the Coefficient of Thermal Expansion

Alloy	Phase	Temperature, °C	Atomic Percent of Phase Composition, Predicted by Thermo-Calc										Caron Model γ Lattice Parameter, Å	Caron Model γ' Lattice Parameter, Å
			Co	Cr	Mo	W	Re	Ru	Al	Ti	Ta	Nb		
N5	γ	982	12.3	15.0	1.1	1.5	1.3	0.0	8.0	0.0	0.4	0.0	3.577	—
N5	γ	1093	10.1	12.5	1.3	1.8	1.4	0.0	10.3	0.0	0.8	0.0	3.584	—
N5	γ'	982	4.6	2.6	0.4	1.1	0.1	0.0	18.2	0.0	3.4	0.0	—	3.590
N5	γ'	1093	4.6	2.5	0.4	1.2	0.1	0.0	18.5	0.0	3.4	0.0	—	3.590
N4	γ	982	10.9	20.8	1.7	2.9	0.0	0.0	4.6	1.3	0.6	0.1	3.589	—
N4	γ	1093	9.0	16.1	1.4	2.4	0.0	0.0	6.8	2.6	1.1	0.2	3.593	—
N4	γ'	982	4.8	2.7	0.2	1.1	0.0	0.0	13.1	6.5	2.2	0.5	—	3.602
N4	γ'	1093	5.0	3.0	0.2	1.0	0.0	0.0	13.4	6.6	2.0	0.5	—	3.602
CMSX4	γ	982	15.8	15.5	0.5	2.0	1.0	0.0	7.0	0.4	0.5	0.0	3.578	—
CMSX4	γ	1093	13.4	12.5	0.6	2.3	1.2	0.0	9.1	0.7	1.0	0.0	3.585	—
CMSX4	γ'	982	6.2	2.3	0.1	1.2	0.1	0.0	16.7	1.9	3.3	0.0	—	3.594
CMSX4	γ'	1093	6.3	2.3	0.1	1.3	0.1	0.0	16.8	1.9	3.5	0.0	—	3.595
PWA1484	γ	982	16.9	11.8	1.6	2.1	1.0	0.0	7.4	0.0	0.7	0.0	3.580	—
PWA1484	γ	1093	14.4	9.6	1.8	2.3	1.3	0.0	9.3	0.0	1.3	0.0	3.588	—
PWA1484	γ'	982	6.1	1.6	0.5	1.1	0.1	0.0	17.4	0.0	4.4	0.0	—	3.595
PWA1484	γ'	1093	6.2	1.6	0.5	1.1	0.1	0.0	17.5	0.0	4.6	0.0	—	3.597

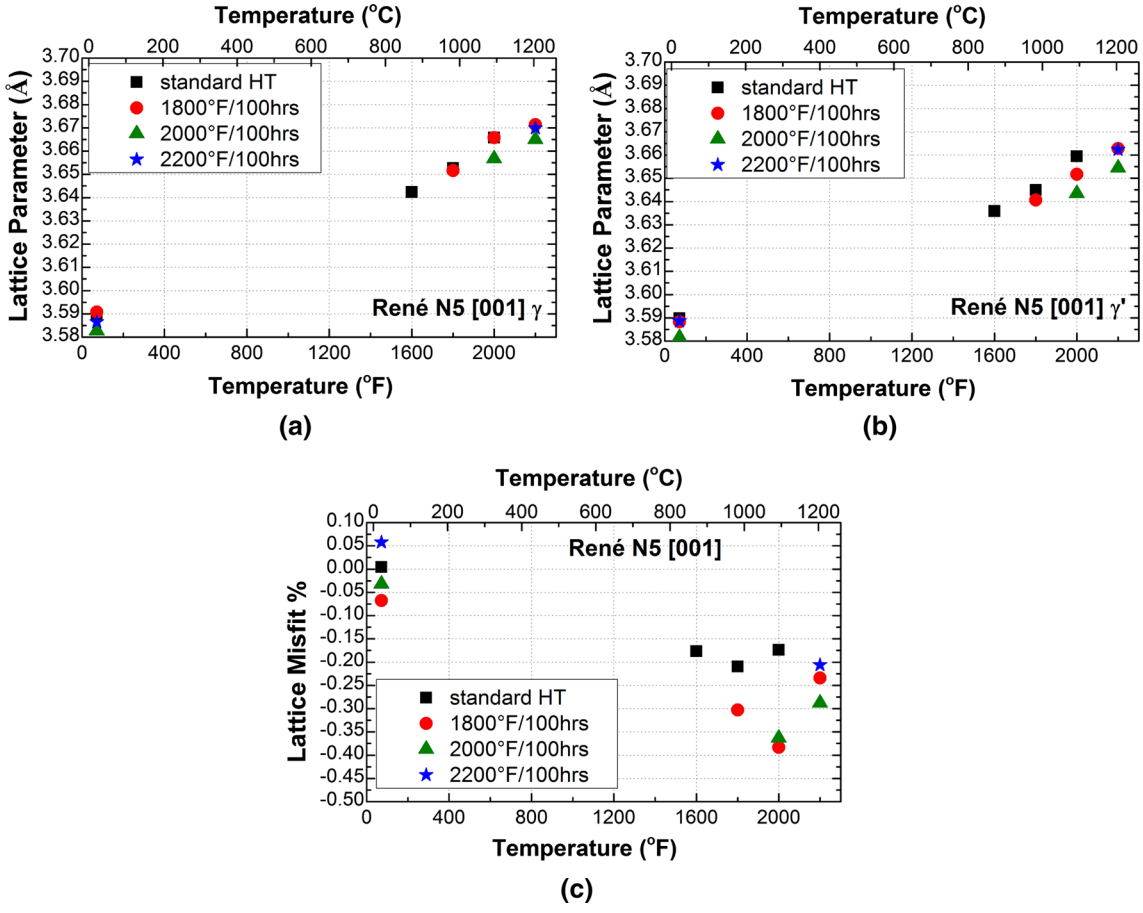

Fig. 7—Comparison of (*a*) γ and (*b*) γ' lattice parameters and (*c*) the misfits for René N5 in the standard heat-treatment condition and 100-h annealed conditions, along the axial [001] direction.

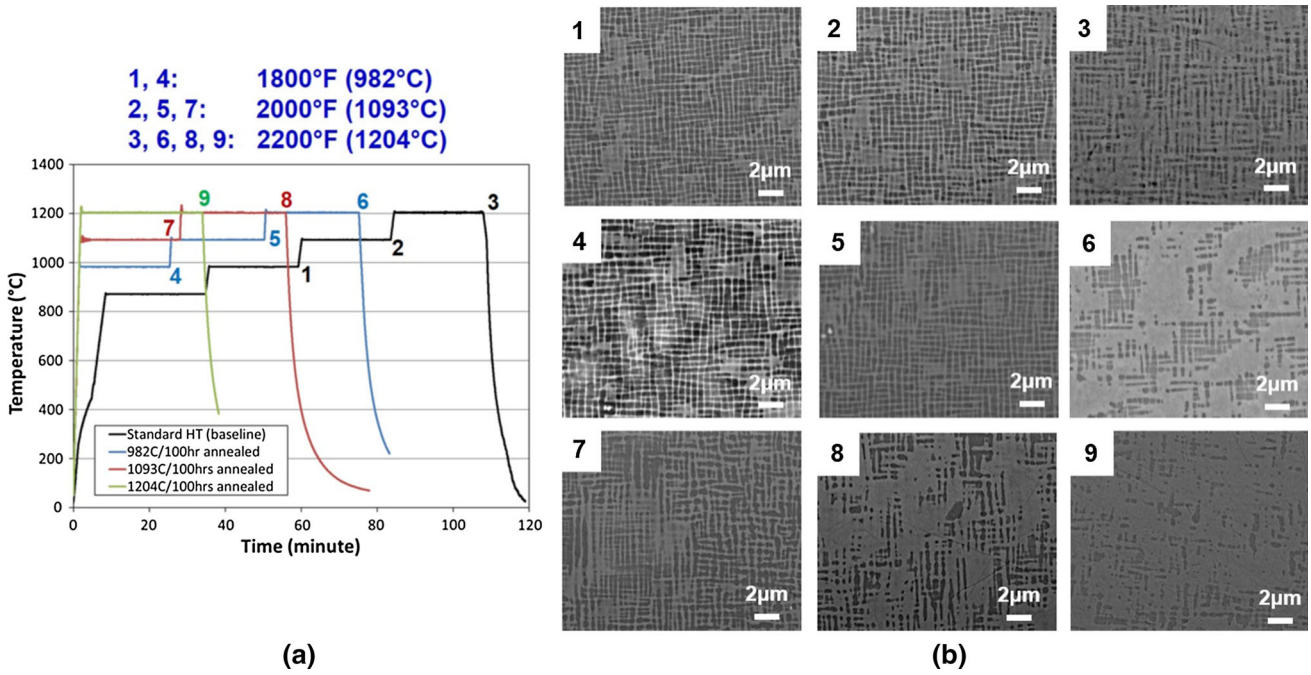

Fig. 8—(*a*) Various heat treatments to mimic each step of the heating profile during the neutron experiment and (*b*) the corresponding microstructure of René N5 after each heat treatment in backscattered electron images. The dark contrast phase is γ' phase, and light contrast phase is γ phase.

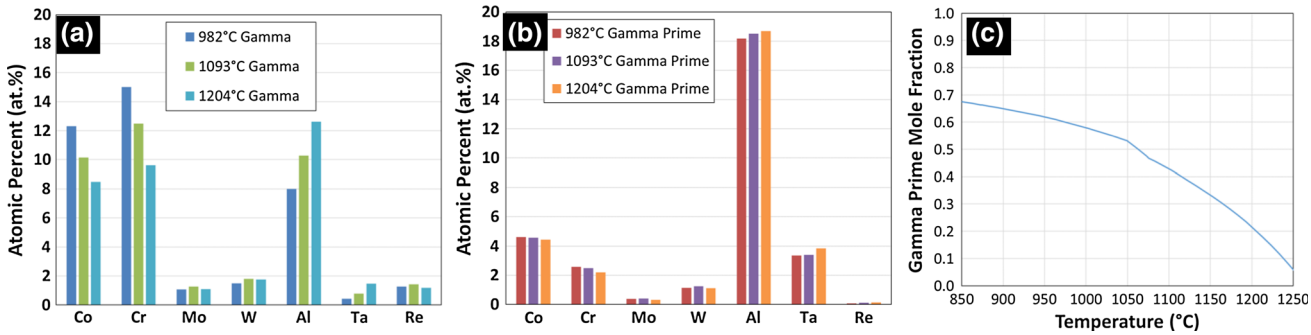

Fig. 9—Thermo-Calc predicted equilibrium composition for (*a*) γ and (*b*) γ' in René N5 and (*c*) the mole fraction of γ' as a function of temperature using the TTNi7 database.

A. *Misfit vs Temperature*

Lattice parameters and misfit along the [001] direction as a function of temperature are shown, respectively, in Figures 5 and 6. All the alloys show smaller lattice parameters for the γ' phase than the γ matrix and negative misfits between 871 °C and 1204 °C. This is indeed consistent with their N-type rafting structure after tensile creep deformation.[32–34] As a function of temperature, CMSX4 shows a monotonic decrease of lattice misfit as a function of temperature, while other alloys exhibit a decrease of lattice misfit up to 1093 °C and then an increase of misfit above that temperature. Many Ni-based single-crystal superalloys, such as CMSX2, SRR99, AM1, CMSX4, and SC16,[4,5,8,10,13,23] show a similar misfit decrease up to 1100 °C. Unfortunately, these measurements did not go beyond 1100 °C. The decrease of misfit can be explained, as the γ has a larger coefficient of thermal expansion than γ'. The observed trend of misfit becoming less negative above 1093 °C for René N4, René N5, and PWA1484 has not been previously reported for other single-crystal superalloys. Such a trend may be related to two factors: the chemistry change in γ and γ' phases or the relaxation of internal stress. To validate these two hypotheses, additional experiments will be required in the future: (1) quantifying the chemistry of the γ and γ' phases at different temperatures and (2) studying the dislocation structure as an indicator of stress relaxation.

The misfit also depends on the alloying effect, *i.e.*, the elemental partitioning between the γ and γ' phases and the corresponding changes of lattice parameters. Based on the partitioning ratio,[5] solid solution elements in the γ phase, such as Re, Cr, Ru, Co, Mo, and W, can alter

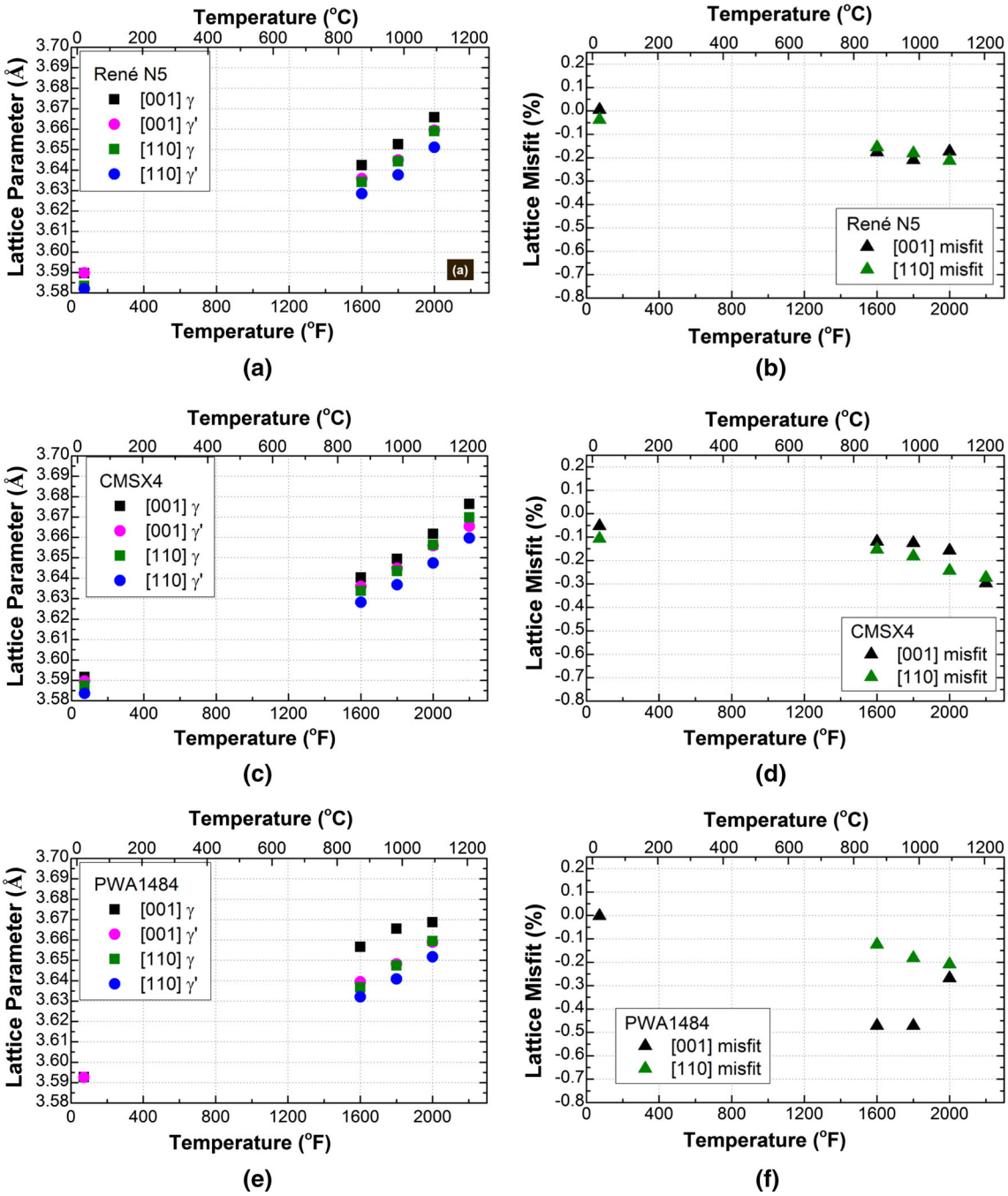

Fig. 10—Lattice parameters and misfit along the axial [001] direction and transverse [011] direction for (*a*) and (*b*) René N5, (*c*) and (*d*) CMSX4, and (*e*) and (*f*) PWA1484.

the γ lattice parameter, while the γ' formers, such as Al, Ta, and Ti, affect the γ' lattice parameter. Pyczak *et al.*[5] studied misfit within a controlled chemistry space and found that Re-containing alloys have more negative misfit at high temperatures in comparison with Re-free alloys. However, current work shows that Re-free René N4 has more negative misfit than alloys containing 3 pct Re (René N5 and CMSX4), although it is comparable with PWA1484 at 871 °C and 982 °C. Among the three alloys containing 3 pct Re, the misfit of PWA1484 is significantly lower than those of René N5 and CMSX4. To our knowledge, for single-crystal Ni-based superalloys, there is no generally accepted model to quantitatively predict the misfit as a function of temperature with the input of composition and thermal expansion coefficients of the γ and γ' phases, and this probably is due to the lack of a large experimental database for model calibration and validation. Caron[37] proposed a room-temperature misfit model considering lattice parameters of pure Ni and pure Ni_3Al, γ and γ' phase

compositions, and Vegard's coefficient of each element. Since Caron's model does not consider the thermal expansion coefficient or temperature effect, only qualitative comparison is made in terms of alloy ranking, assuming coefficients of thermal expansion of the γ and γ' phases are quite close among the four alloys. Thermo-Calc with the TTNi7 database was used to obtain γ and γ' compositions for the four alloys. As shown in Table II, the model results suggest γ lattice parameter in the order of René N4 > PWA1484 > CMSX4 > René N5, while our experimental data show the order of René N4 > PWA1484 > René N5 > CMSX4. The model results suggest γ' lattice parameter also in the order of René N4 > PWA1484 > CMSX4 > René N5, while our experimental data show the order of René N4 > PWA1484 > CMSX4 and René N5. Thus, there is good agreement between this model and experiments. Although René N4 has 0 Re, it has a higher amount of Cr, Ti, and Mo in the γ phase compared to the other three alloys. Those elements have a high Vegard's coefficient leading to a larger lattice parameter.

B. *Effect of Annealing on Misfit*

To evaluate the misfit evolution during thermal exposure, three René N5 specimens were annealed at 982 °C, 1093 °C, and 1204 °C, respectively, for 100 hours and were measured by neutron diffraction at and above the annealing temperature. The results are compared with the René N5 sample after the standard heat treatment. For example, for the sample annealed at 982 °C, the neutron measurements were at 982 °C, 1093 °C, and 1204 °C, and for the sample annealed at 1093 °C, the neutron measurements were at 1093 °C and 1204 °C. The room-temperature measurements were always carried out for these samples. The lattice parameters and misfits based on the data from bank 1 are displayed in Figure 7. After annealing, both γ and γ' lattice parameters become smaller and the reduction is greater for γ' than for γ. Therefore, more negative misfit is observed after annealing compared to the standard heat-treatment conditions. This may be associated with one of the two microstructural events: loss of coherency between the γ and γ', leading to high magnitude of misfit or chemistry change in γ and γ'.

To understand the microstructural status at each isothermal step during the *in-situ* neutron measurements, a set of nine René N5 samples were first heat treated and water quenched and then examined by SEM. The heat-treatment conditions were designed so that the microstructure of the water-quenched sample will resemble the high-temperature microstructure at which the neutron measurement was made. Detailed heat treatments for the nine samples are described subsequently:

(1) standard heat treatment (HT) + 871 °C 25 minutes + 982 °C 25 minutes + water quench (WQ)
(2) standard HT + 871 °C 25 minutes + 982 °C 25 minutes + 1093 °C 25 minutes + WQ
(3) standard HT + 871 °C 25 minutes + 982 °C 25 minutes + 1093 °C 25 minutes + 1204 °C 25 minutes + WQ
(4) 982 °C 100 hour + 982 °C 25 minutes + WQ
(5) 982 °C 100 hour + 982 °C 25 minutes + 1093 °C 25 minutes + WQ
(6) 982 °C 100 hour + 982 °C 25 minutes + 1093 °C 25 minutes + 1204 °C 25 minutes + WQ
(7) 1093 °C 100 hour + 1093 °C 25 minutes + WQ
(8) 1093 °C 100 hour + 1093 °C 25 minutes + 1204 °C 25 minutes + WQ
(9) 1204 °C 100 hour + 1204 °C 25 minutes + WQ

Representative SEM images of these nine samples and the heat-treatment conditions are given in Figure 8. For example, sample 1 is used to reproduce the microstructure of René N5 at 982 °C after its standard heat treatment, sample 9 is used to reproduce the microstructure of René N5 at 1204 °C after annealing at 1204 °C for 100 hours, and so on.

For the samples after the standard heat treatment and the samples after annealing at 982 °C, the γ/γ' interfacial coherency is retained up to 1093 °C, as shown in images 1 and 2 for the former and 4 and 5 for the latter. After exposure at temperatures above 1093 °C, both groups of samples showed reduced volume fraction of the γ' particles and loss of cuboidal shape in the γ' precipices due to the dissolution of γ' and loss of interfacial coherency (in the ascending order 3, 7, 8, 6, and 9). A finite-element model to understand internal stress at the γ and γ' phases will be necessary in future work to further understand internal stress evolution and loss of coherency during anneal.

Chemistry evolution in the γ and γ' phases was not directly measured in the current study but was estimated by Thermo-Calc equilibrium phase prediction using the TTNi7 database. It is assumed that the alloy after 100 hour annealing is close to the equilibrium state. As presented in Figure 9, the γ' mole fraction decreases from 60 to 21 pct when the temperature increases from 982 °C to 1204 °C, which is consistent with our observation of the decrease in γ' superlattice peak intensity at higher temperatures. A larger change in the γ phase chemistry is found with increasing temperature than that in the γ' chemistry, which shows qualitative agreement with the measurements in a similar type of superalloy containing 3 pct Re.[36] Reduced Co and Cr and increased Al are predicted in the γ matrix with increasing temperature and the γ' dissolution.

However, the γ' phase composition only shows marginal change with increasing temperature. Since the γ and γ' lattice parameters show similar magnitude of change after annealing (Figure 7), it is likely that the loss of coherency in combination with the change of chemistry is responsible for the γ' lattice parameter change after a 100-hour anneal.

Pyczak[5] also reported more negative misfits for a few single-crystal alloys at room temperature after 1000 °C/500 hour annealing, although the magnitude of misfit change varies from alloy to alloy. Such a change was ascribed to a dislocation network at the γ/γ' interface, resulting in tensile stress in γ and compressive stress in γ'. Our room-temperature data after 982 °C/100 hour anneal show a similar trend of increase in γ and decrease

in γ' lattice parameters when compared to those before anneal, while the data at both 1093 °C and 1204 °C display a decrease in γ and γ' lattice parameters, which is not consistent with Reference 5. It should be emphasized that larger uncertainty (± 0.1 pct) of misfit can be seen when misfit is small (close to zero), due to the limited angular resolution and the difficulty to deconvolute γ/γ' peaks. As shown in Figure 7(c), at room temperature, all the misfits are close to zero within ± 0.1 pct. Therefore, the true trend is not clearly seen to be compared with Reference 5. Also, to confirm whether the dislocation network has formed in the annealed René N5 samples, additional TEM characterization is required in future work.

C. *Misfit Anisotropy in Different Crystal Orientations (Sample Axial/Transverse Direction)*

The lattice parameters and misfit in the axial and the transverse directions are found to be slightly different, suggesting that the misfit is anisotropic with respect to the crystal orientation. For René N5, CMSX4, and PWA1484, the γ and γ' lattice parameters along the axial direction are larger than those along the transverse direction (Figure 10). This trend is not caused by instrument alignment/calibration, because the standard Si powders show the same lattice parameters in the two directions. For PWA1484, a larger discrepancy between the γ lattice parameters is found from the 871 °C and 982 °C data. As a result, PWA1484 shows less negative misfit along the transverse direction than the axial direction. In contrast, CMSX4 shows slightly more negative misfit along the transverse direction, except for 1204 °C, and René N5 shows comparable misfits in both directions. Therefore, the degree of anisotropy appears in the order of PWA1484 > CMSX4 > René N5.

The anisotropic behavior of misfit suggests a tetragonal distortion for the pseudo-cubic unit cells of both the γ and γ' phases. In fact, the tetragonal distortion in the γ phase has been observed by X-ray diffraction, in which slightly different lattice parameters were found between horizontal and vertical γ channels.[10,14,15] However, tetragonal distortion in the γ' phases is rarely described in the literature. Reference 30 confirmed misfit anisotropy for both γ and γ' in single-crystal superalloy DD10 and stated that the heat treatment with improved chemistry homogeneity caused the lattice distortion and such a distortion did not exist in the as-cast condition with chemistry inhomogeneity. References 7 and 35 reported the γ' tetragonality by using both γ-ray diffractometry and neutron diffraction and concluded that the temporal evolution of tetragonality depends on thermal history and internal stress.

A possible cause of tetragonal distortion and misfit anisotropy could be either internal stress on the γ and γ' phases or chemistry inhomogeneity on the dendritic structure. The casting process produces primary dendrite grown along the [001] direction, and secondary dendrite grown along the [010] and [001] directions. The internal stress states along the primary and secondary dendrite arms may be different. In addition, chemistry inhomogeneity exists in the DC and IDR after casting. Although solution treatment can largely reduce the chemical inhomogeneity, some degree of chemical segregation in the DC and IDR is known to be present after the heat treatment. A slight difference in the lattice parameters between the DC and the IDRs is expected due to the chemistry segregation. Therefore, the bulk averaged lattice parameters along the primary dendrite growth direction and transverse direction could be different due to different fractions of IDR in the sampling volume. To better understand the origin of tetragonal distortion, studies on the effect of internal stress, phase chemistry, and microstructure evolution on lattice misfit, from as-cast to solution and aging states, will be required in the future.

IV. CONCLUSIONS

TOF neutron diffraction is a suitable method for measuring lattice misfit for single-crystal superalloy samples of centimeter size. Still, when the misfit is small, say, less than ± 0.1 pct, and there is lack of visible separation between the γ and γ' peaks, accurate determination of the misfit can be a challenge. The data analysis method can also affect the misfit values given the same data, mainly through the peak shape function used in the analysis and if such functions are constrained between the γ and γ' peaks.

For a specific single-crystal superalloy, misfit is influenced by multiple factors, including chemistry, γ/γ' interfacial coherency, heat-treatment history, crystal orientation, internal stress, probing volume, and location (DC, IDR, or bulk). All the alloys studied in this work show negative misfit at temperatures above 871 °C. For most alloys, the misfit becomes less negative at temperatures above 1093 °C, possibly due to either chemistry effect or internal stress relaxation. The magnitude of γ and γ' lattice parameters in the studied four alloys shows a qualitative agreement with a misfit model based on Vegard's coefficients. Re-free alloy could have a larger γ lattice parameter and γ/γ' misfit than the three alloys containing 3 pct Re when other elements with higher Vegard's coefficients come into play, such as Cr, Ti, and Mo in René N4. Misfit anisotropy, being present in several alloys, could be due to internal stress induced by either the casting process or chemistry segregation at DC and IDR. René N5 shows more negative misfit after 100 hours of annealing at high temperatures than after standard heat treatment. Comparison between as heat treated and after annealing provides insight into the misfit evolution during high-temperature exposure.

ACKNOWLEDGMENTS

The authors from General Electric acknowledge the support from Steven Duclos, Bernard Bewlay, Margaret Blohm, and P.R. Subramanian. The authors are also grateful to Chris McLasky and Mike Knussman, GRC, and Matt Frost, ORNL, for their technical support, and Ning Zhou, Mallikarjun Karadge, and Chen

Shen, GRC, for technical discussion. This research used resources at the Spallation Neutron Source, a DOE Office of Science User Facility operated by the Oak Ridge National Laboratory.

REFERENCES

1. R.A. Ricks, A.J. Porter, and R.C. Ecob: *Acta Metall.*, 1983, vol. 31, pp. 43–53.
2. F.R.N. Nabarro: *Metall. Mater. Trans. A*, 1996, vol. 27A, pp. 513–30.
3. E.M. Francis, B.M.B. Grant, J. Quinta da Fonseca, P.J. Phillips, M.J. Mills, M.R. Daymond, and M. Preuss: *Acta Mater.*, 2014, vol. 74, pp. 18–29.
4. D. Sieborger, H. Brehm, F. Wunderlich, D. Moller, and U. Galtzel: *Z. Metallkd.*, 2001, vol. 92, pp. 58–61.
5. F. Pyczak, B. Devrient, and H. Mughrabi: *Superalloys 2004,* Proc. 10th Int. Symp. on Superalloys, TMS, Warrendale, PA, 2004, pp. 827–36.
6. Y. Lu, S. Ma, and B.S. Majumdar: *Superalloys 2008,* Proc. 11th Int. Symp. on Superalloys, TMS, Warrendale, PA, 2008, pp. 553–62.
7. D. Bellet and P. Bastie: *Philos. Mag. B*, 1991, vol. 64, pp. 143–52.
8. H. Biermann, M. Strehler, and H. Mughrabi: *Metall. Mater. Trans. A*, 1996, vol. 27A, pp. 1003–14.
9. U. Bruckner, A. Epishin, T. Link, and K. Dressel: *Mater. Sci. Eng. A*, 1998, vol. 247, pp. 23–31.
10. G. Bruno, G. Schumacher, and H. Cavalcanti: *Metall. Mater. Trans. A*, 2003, vol. 34A, p. 193.
11. G. Bruno and H. Cavalcanti Pinto: *Superalloys 2004,* Proc. 10th Int. Symp. on Superalloys, TMS, Warrendale, PA, 2004, pp. 837–46.
12. J. Coakley, R.C. Reed, J.L.W. Warwick, K.M. Rahman, and D. Dye: *Acta Mater.*, 2012, vol. 60, pp. 2729–38.
13. L. Dirand, J. Cormier, A. Jacques, J. Chateau-Cornu, T. Schenk, O. Ferry, and P. Bastie: *Mater. Character.*, 2013, vol. 77, pp. 32–46.
14. A. Jacques, F. Diologent, and P. Bastie: *Mater. Sci. Eng. A*, 2004, vol. 387, pp. 944–49.
15. H.A. Kuhn, H. Biermann, T. Ungar, and H. Mughrabi: *Acta Metall. Mater.*, 1991, vol. 39, pp. 2783–94.
16. J. Le Graverend, L. Dirand, A. Jacques, J. Cormier, O. Ferry, T. Schenk, F. Gallerneau, S. Kruch, and J. Mendez: *Metall. Mater. Trans. A*, 2012, vol. 43A, pp. 3946–51.
17. T. Link, A. Epishin, U. Bruckner, and P. Portella: *Acta Mater.*, 2000, vol. 48, pp. 1981–94.
18. H. Mughrabi, H. Biermann, and T. Ungar: *Superalloys 1992,* Proc. 7th Int. Symp. on Superalloys, TMS, Warrendale, PA, 1992, pp. 599–608.
19. A. Royer, P. Bastie, D. Bellet, and J.L. Strudel: *Philos. Mag. A*, 1995, vol. 72, pp. 669–89.
20. A. Royer, P. Bastie, and M. Veron: *Acta Mater.*, 1998, vol. 46, pp. 5357–68.
21. G. Schumacher, N. Darowski, I. Zizak, H. Klingelhoffer, and W. Neumann: *Scripta Mater.*, 2009, vol. 60, pp. 88–91.
22. F. Diologent, P. Caron, T. d'Almeida, S. Chambreland, A. Jacques, and P. Bastie: *Int. J. Mater. Res.*, 2006, vol. 97, pp. 1136–42.
23. M. Fährmann, J.G. Wolf, and T.M. Pollock: *Mater. Sci. Eng. A*, 1996, vol. 210, pp. 8–15.
24. R. Gilles, D. Mukherji, M. Hoelzel, P. Strunz, D.M. Toebbens, and B. Barbier: *Acta Mater.*, 2006, vol. 54, pp. 1307–16.
25. R. Gilles, D. Mukherji, D. Del Genovese, P. Strunz, B. Barbier, W. Kockelmann, J. Rosler, and H. Fuess: *Mater. Sci. Forum*, 2003, vols. 426–432, pp. 821–28.
26. X.G. Liu, L. Wang, L.H. Lou, and J. Zhang: *J. Mater. Sci. Technol.*, 2015, vol. 31, pp. 143–47.
27. J.P. Minshull, S. Neumeier, M.G. Tucker, and H.J. Stone: *Adv. Mater. Res.*, 2011, vol. 278, pp. 399–404.
28. S. Neumeier, J. Ang, R.A. Hobbs, C.M.F. Rae, and H.J. Stone: *Adv. Mater. Res.*, 2011, vol. 278, pp. 60–65.
29. F. Pyczak, S. Neumeier, and M. Goken: *Mater. Sci. Eng., A,* 2009, vols. 510–511, pp. 295–300.
30. E. Wu, G. Sun, B. Chen, T. Pirling, D.J. Hughes, S. Wang, and J. Zhang: *Acta Mater.*, 2013, vol. 61, pp. 2308–19.
31. K. An, H.D. Skorpenske, A.D. Stoica, D. Ma, X.L. Wang, and E. Cakmak: *Metall. Mater. Trans. A*, 2011, vol. 42A, pp. 95–99.
32. L.H. Rettberg, M. Tsunekane, and T.M. Pollock: *Superalloys 2012,* Proc. 12th Int. Symp. on Superalloys, TMS, Warrendale, PA, 2012, pp. 341–49.
33. C.G. Shastry, V.S.G. Kelekanjeri, T. Vishwanath, and S. Chaudhuri: *Mater. Sci. Eng. A*, 2013, vol. 585, pp. 47–56.
34. N. Matan, D.C. Cox, C.M.F. Rae, and R.C. Reed: *Acta Mater.*, 1999, vol. 47, pp. 2031–45.
35. D. Bellet and P. Bastie: *Philos. Mag. B*, 1991, vol. 64, pp. 135–41.
36. F. Pyczak, S. Neumeier, and M. Göken: *Mater. Sci. Eng. A*, 2010, vol. 527, pp. 7939–43.
37. P. Caron: *Superalloys 2000,* Proc. 9th Int. Symp. on Superalloys, TMS, Warrendale, PA, 2000, pp. 737–46.
38. G. Bruno, H.C. Pinto, and W. Reimers: *Appl. Phys. A*, 2002, vol. 74, pp. S940–S942.
39. G. Bruno and H.C. Pinto: *Mater. Sci. Technol.*, 2003, vol. 19, pp. 567–72.
40. H.C. Pinto and G. Bruno: *J. Synchrotron Rad.*, 2003, vol. 10, pp. 148–53.
41. J. Coakley, E.A. Lass, D. Ma, M. Frost, and D.N. Seidman: *Scripta Mater.*, 2017, vol. 134, pp. 110–14.
42. J. Coakley, D. Ma, M. Frost, D. Dye, D.N. Seidman, D.C. Dunand, and H.J. Stone: *Acta Mater.*, 2017, vol. 135, pp. 77–87.
43. G. Bruno, B. Schönfeld, and G. Kostorz: *Z. Metallkd.*, 2003, vol. 94, pp. 12–18.